Science Advances
AAAS

Supplementary Materials for

Molecular ruler mechanism and interfacial catalysis of the integral membrane acyltransferase PatA

Itxaso Anso, Luis G. M. Basso, Lei Wang, Alberto Marina, Edgar D. Páez-Pérez, Christian Jäger, Floriane Gavotto, Montse Tersa, Sebastián Perrone, F.-Xabier Contreras, Jacques Prandi, Martine Gilleron, Carole L. Linster, Francisco Corzana, Todd L. Lowary, Beatriz Trastoy*, Marcelo E. Guerin*

*Corresponding author. Email: beatriz.trastoy@gmail.com (B.T.); mrcguerin@gmail.com (M.E.G.)

Published 15 October 2021, *Sci. Adv.* **7**, eabj4565 (2021)
DOI: 10.1126/sciadv.abj4565

This PDF file includes:

1. SUPPLEMENTARY METHODS

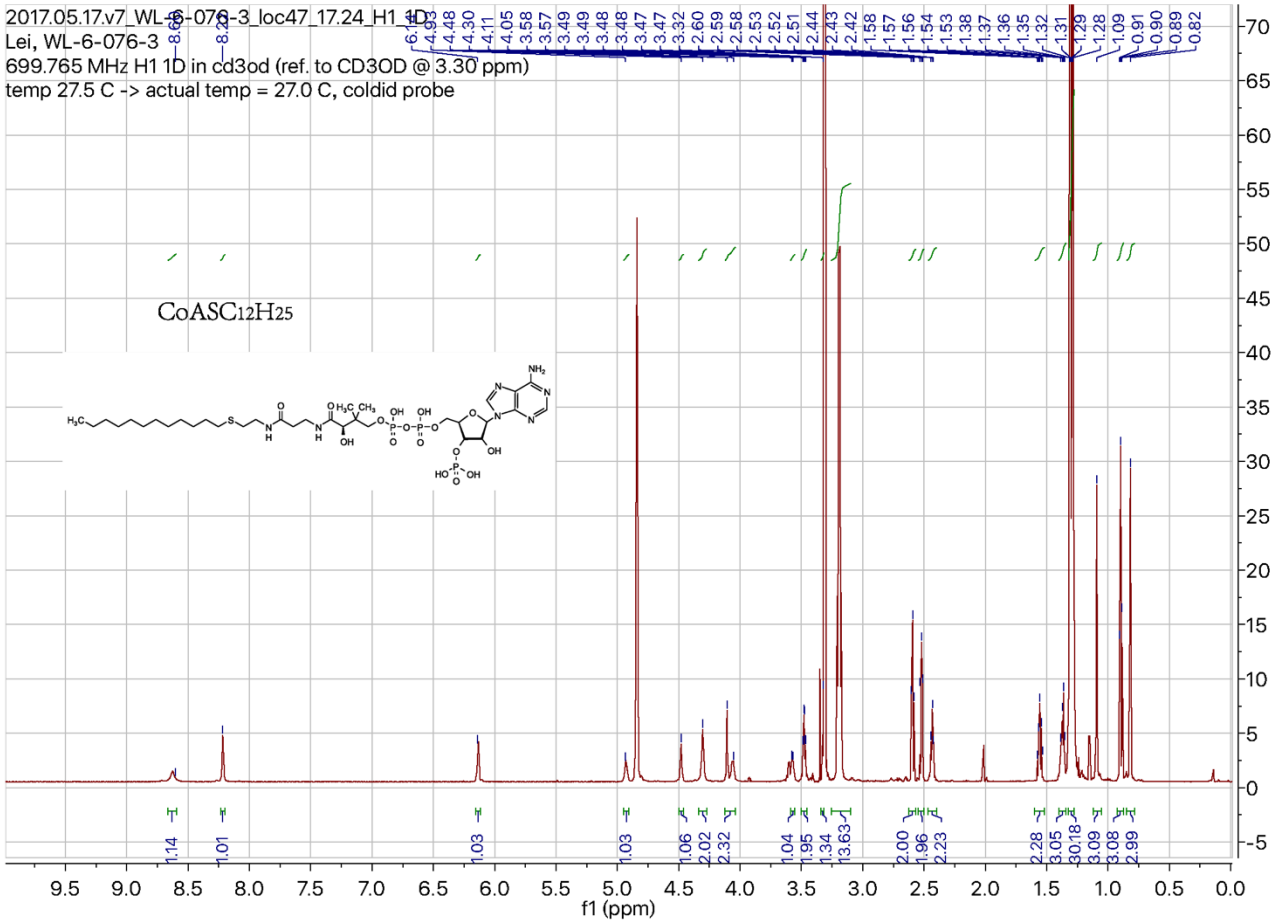

Data for S-C12-CoA product: (11 mg product from 60 mg CoA, 11% yield). $_1$H NMR (700 MHz, CD_3OD, δ_H) 8.63 (s, 1 H), 8.22 (s, 1 H), 6.14 (d, 1 H, J = 6.0 Hz), 4.93 (brs, 1 H), 4.83-4.80 (m, 1 H), 4.48 (s, 1 H), 4.30 (brs, 2 H), 4.10 (s, 1 H), 4.06 (d, 1 H, J = 10.5 Hz), 3.57 (d, 1 H, J = 9.5 Hz), 3.48 (td, 2 H, J = 7.0, 2.0 Hz), 3.32 (t, 3 H, J = 7.2 Hz), 3.19 (q, 16 H, J = 6.7 Hz), 2.59 (t, 2 H, J = 7.2 Hz), 2.52 (t, 2 H, J = 7.2 Hz), 2.43 (td, 2 H, J = 7.2, 1.5 Hz), 1.57-1.53 (m, 2 H), 1.39-1.27 (m, 18 H), 1.31 (t, 3 H, J = 6.7 Hz), 1.09 (s, 3 H), 0.90 (t, 3 H, J = 7.2 Hz), 0.82 (s, 3 H). HRMS (ESI) calcd for $(M–2H)^{-2}$ $C_{33}H_{58}N_7O_{16}P_3S$: 466.6442. Found: 466.6433.

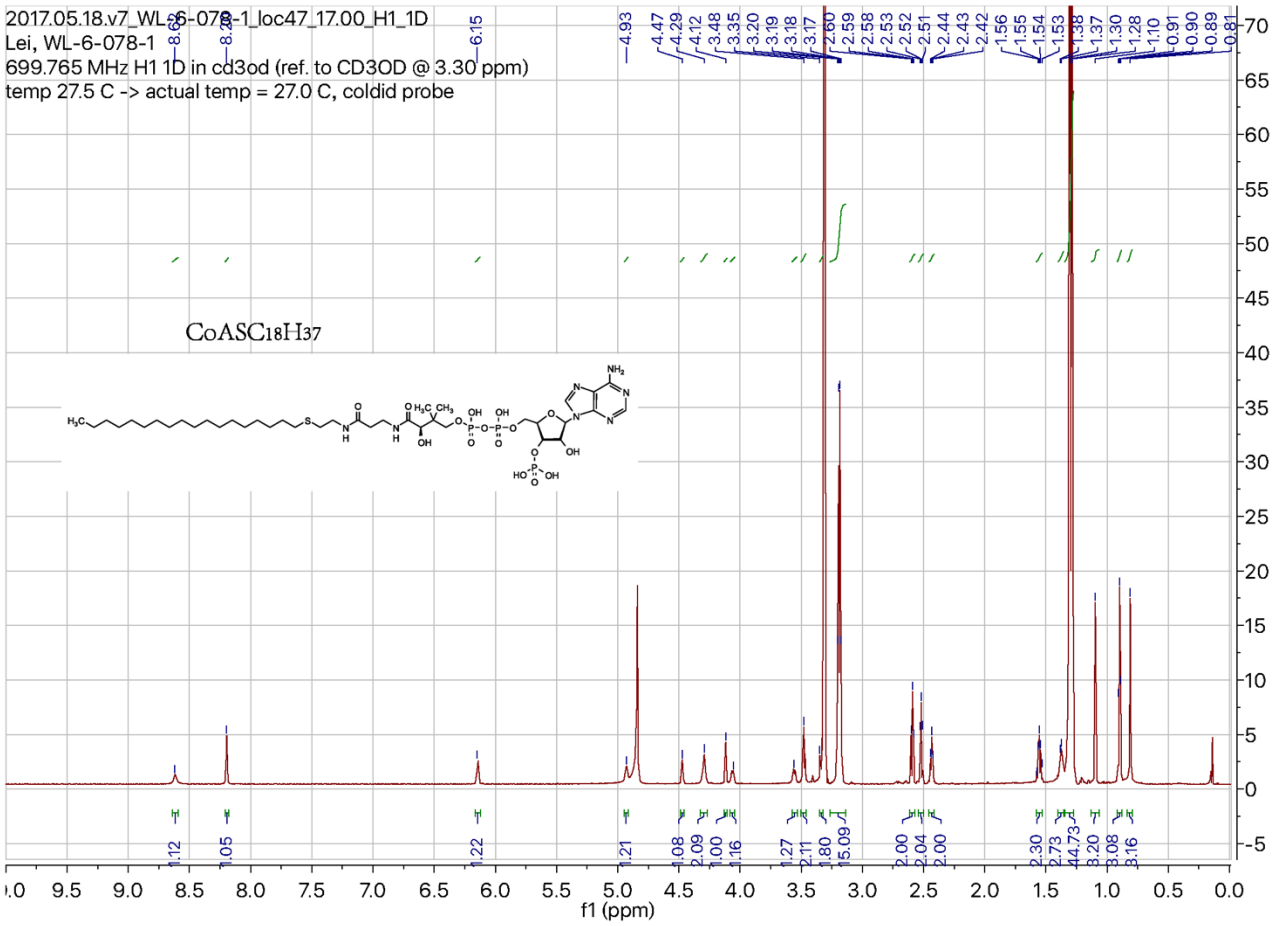

Data for S-C18-CoA product: (10 mg product from 60 mg CoA, 12% yield). ^{1}H NMR (700 MHz, CD_3OD, δ_H) 8.63 (s, 1 H), 8.20 (s, 1 H), 6.14 (d, 1 H, J = 6.0 Hz), 4.93 (brs, 1 H), 4.88 (brs, 1 H), 4.47 (s, 1 H), 4.29 (brs, 2 H), 4.12 (s, 1 H), 4.06 (d, 1 H, J = 9.0 Hz), 3.56 (d, 1 H, J = 8.5 Hz), 3.49 (t, 2 H, J = 7.0 Hz), 3.32 (t, 3 H, J = 7.2 Hz), 3.19 (q, 16 H, J = 6.7 Hz), 2.59 (t, 2 H, J = 7.2 Hz), 2.52 (t, 2 H, J = 7.2 Hz), 2.43 (t, 2 H, J = 7.2 Hz), 1.57-1.53 (m, 2 H), 1.39-1.27 (m, 18 H), 1.31 (t, 3 H, J = 6.7 Hz), 1.09 (s, 3 H), 0.90 (t, 3 H, J = 7.2 Hz), 0.82 (s, 3 H). HRMS (ESI) calcd for $(M–2H)^{-2}$ $C_{39}H_{70}N_7O_{16}P_3S$: 508.6912. Found: 508.6903.

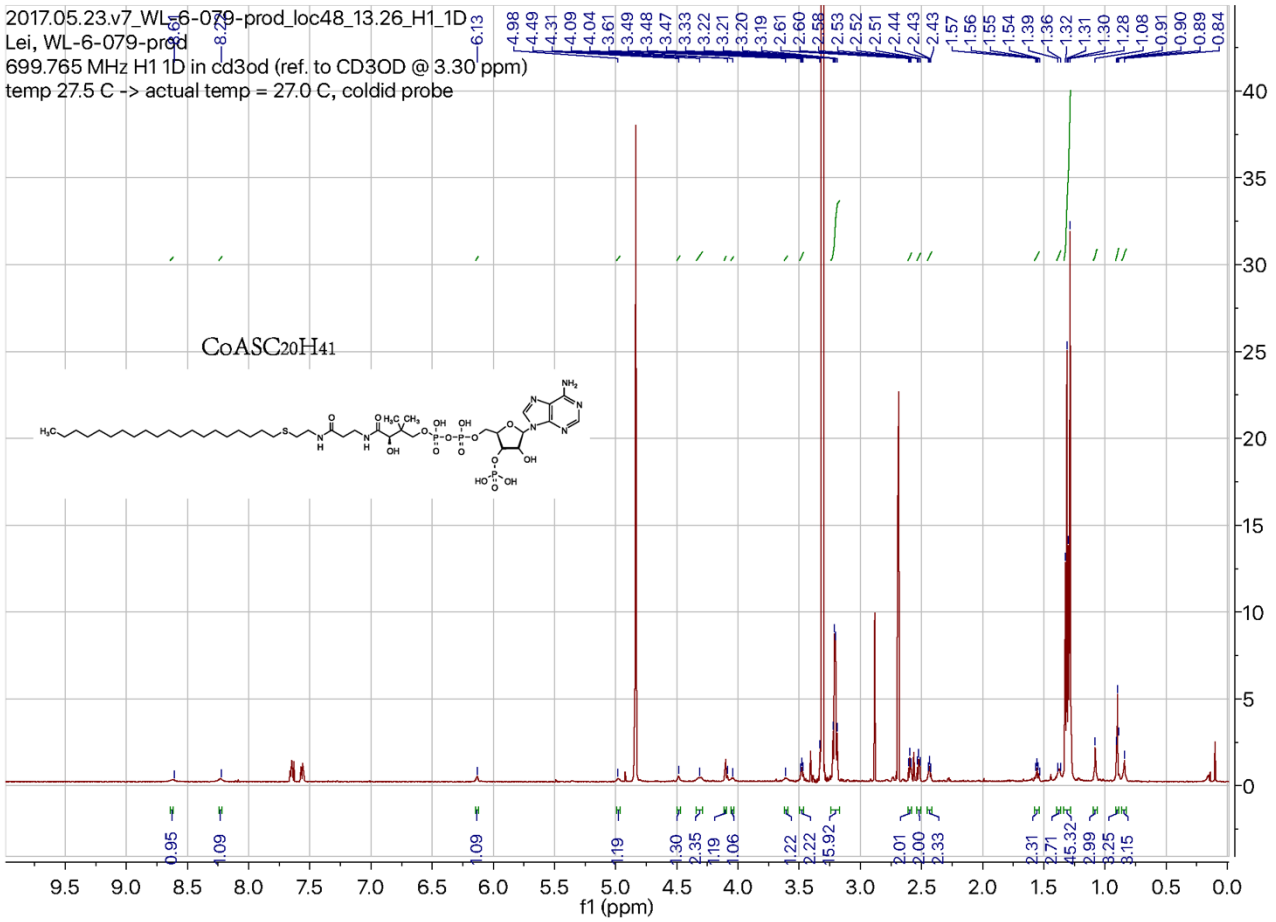

Data for S-C20-CoA product: (2 mg product from 60 mg CoA, 2.4% yield). $_1$H NMR (700 MHz, CD_3OD, δ_H) 8.62 (s, 1 H), 8.23 (s, 1 H), 6.13 (d, 1 H, J = 6.0 Hz), 4.98 (brs, 1 H), 4.84 (brs, 1 H), 4.49 (s, 1 H), 4.31 (brs, 2 H), 4.10 (s, 1 H), 4.05 (d, 1 H, J = 9.0 Hz), 3.61 (d, 1 H, J = 8.5 Hz), 3.48 (t, 2 H, J = 7.0 Hz), 3.32 (t, 3 H, J = 7.2 Hz), 3.19 (q, 16 H, J = 6.7 Hz), 2.59 (t, 2 H, J = 7.2 Hz), 2.52 (t, 2 H, J = 7.2 Hz), 2.43 (t, 2 H, J = 7.2 Hz), 1.57-1.53 (m, 2 H), 1.39-1.27 (m, 18 H), 1.31 (t, 3 H, J = 6.7 Hz), 1.09 (s, 3 H), 0.90 (t, 3 H, J = 7.2 Hz), 0.82 (s, 3 H). HRMS (ESI) calcd for $M–2H)^{-2}$ $C_{41}H_{74}N_7O_{16}P_3S$: 522.7068. Found: 522.7061.

Supplementary Figures

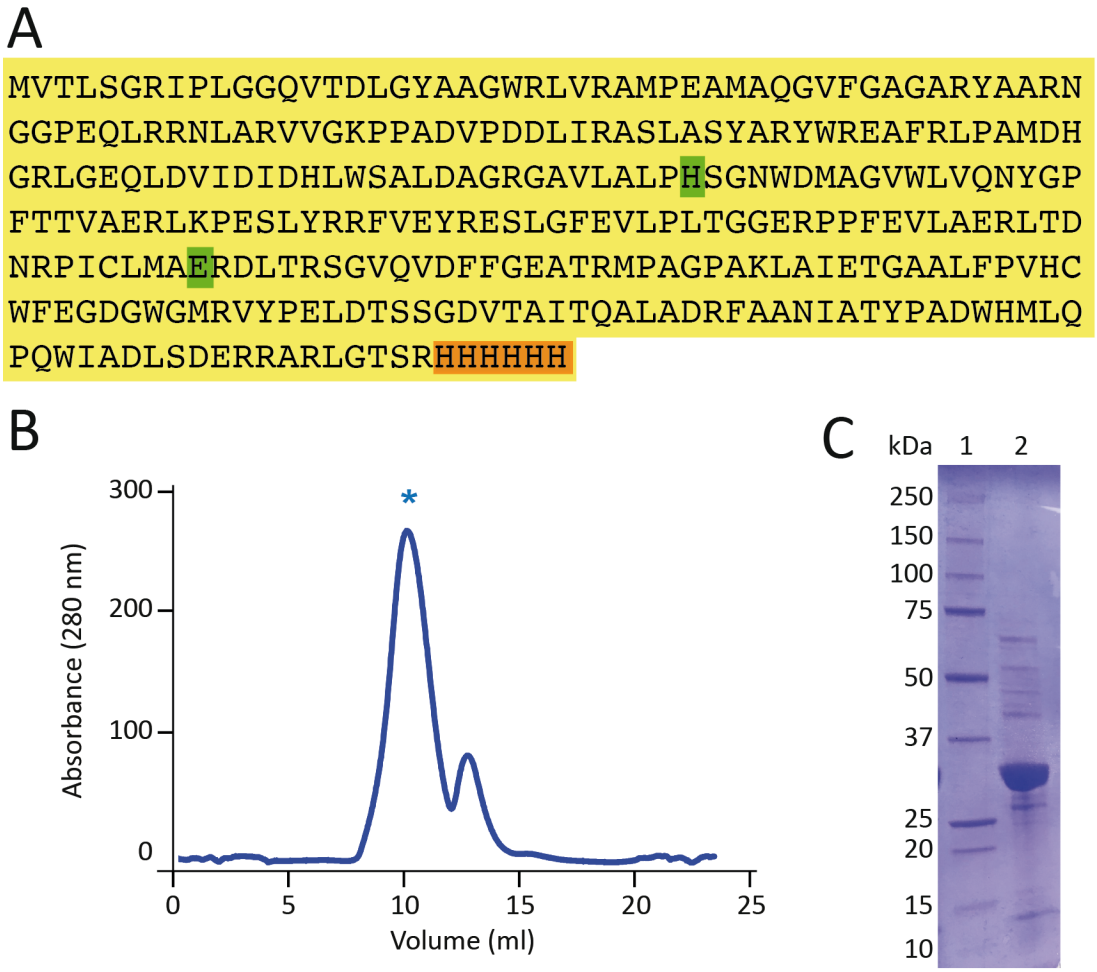

Fig. S1. Recombinant production of full length PatA from *M. smegmatis*. (A) The recombinant full length PatA construct is highlighted in yellow. Catalytic residues are highlighted in green and his-tag in orange. **(B)** Superdex 200 Increase 10/300 GL profile showing the purified full length PatA. **(C)** SDS-PAGE showing the purified full length PatA. The sample was run in one gel.

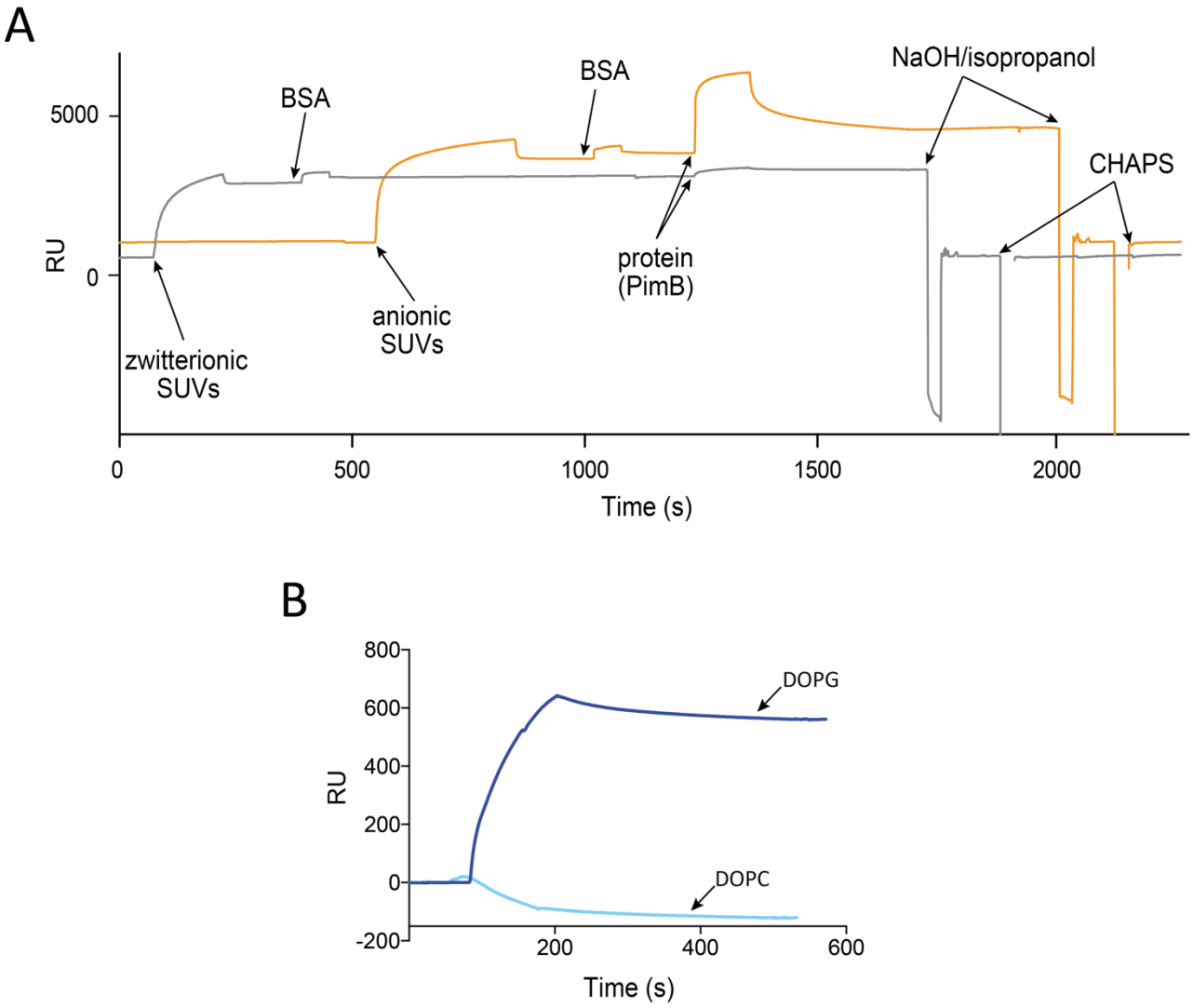

Fig. S2. SPR binding experiments of PatA and SUVs. (A) Sensograms of flow cell 1 (Fc1; grey) and flow cell 2 (Fc2; orange) chip surfaces, highlighting the lipid capture (injection of zwitterionic and anionic SUVs, respectively), binding interaction (protein association and dissociation events) and regeneration (injection of NaOH/Isopropanol and the detergent CHAPS) steps. (B) SPR sensograms of 4.5 µM of PatA showing no binding with DOPC-SUVs (light blue) and binding event with DOPG-SUVs (dark blue).

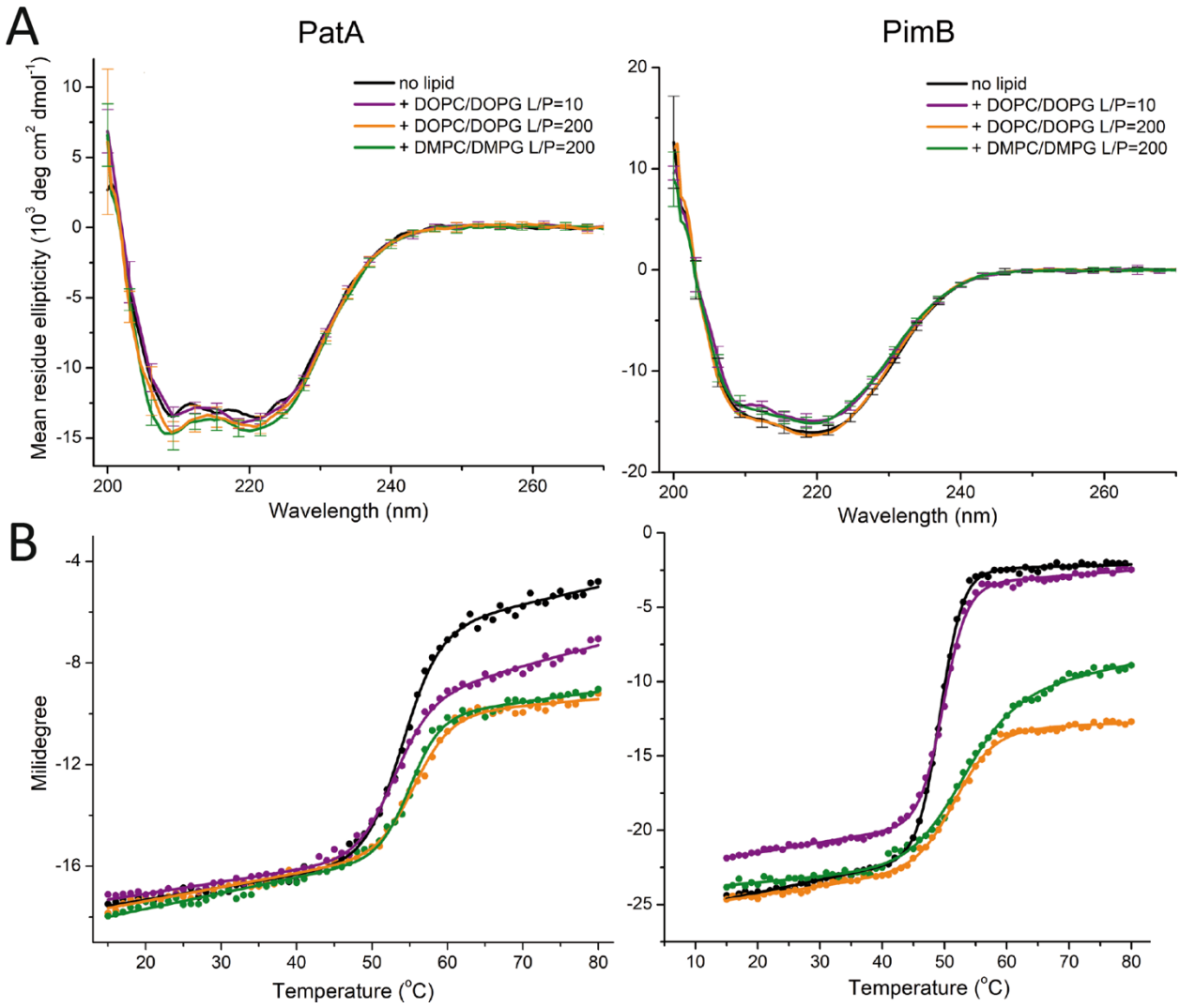

Fig. S3. Secondary structure and thermal stability of PatA and PimB in the presence of lipids. **(A)** Far-UV CD spectra recorded at 20 ºC and **(B)** ellipticity at 222 nm as a function of temperature for PatA (left) and PimB (right) in the absence and presence of DOPC/DOPG 40:60 SUVs and DMPC/DMPG 40:60 SUVs at the lipid-to-protein ratios (L/P) indicated. Solid lines are best fits to the CD data using a two-state equilibrium model. The thermodynamic parameters of the protein unfolding transition are summarized in the Supplementary Table S1.

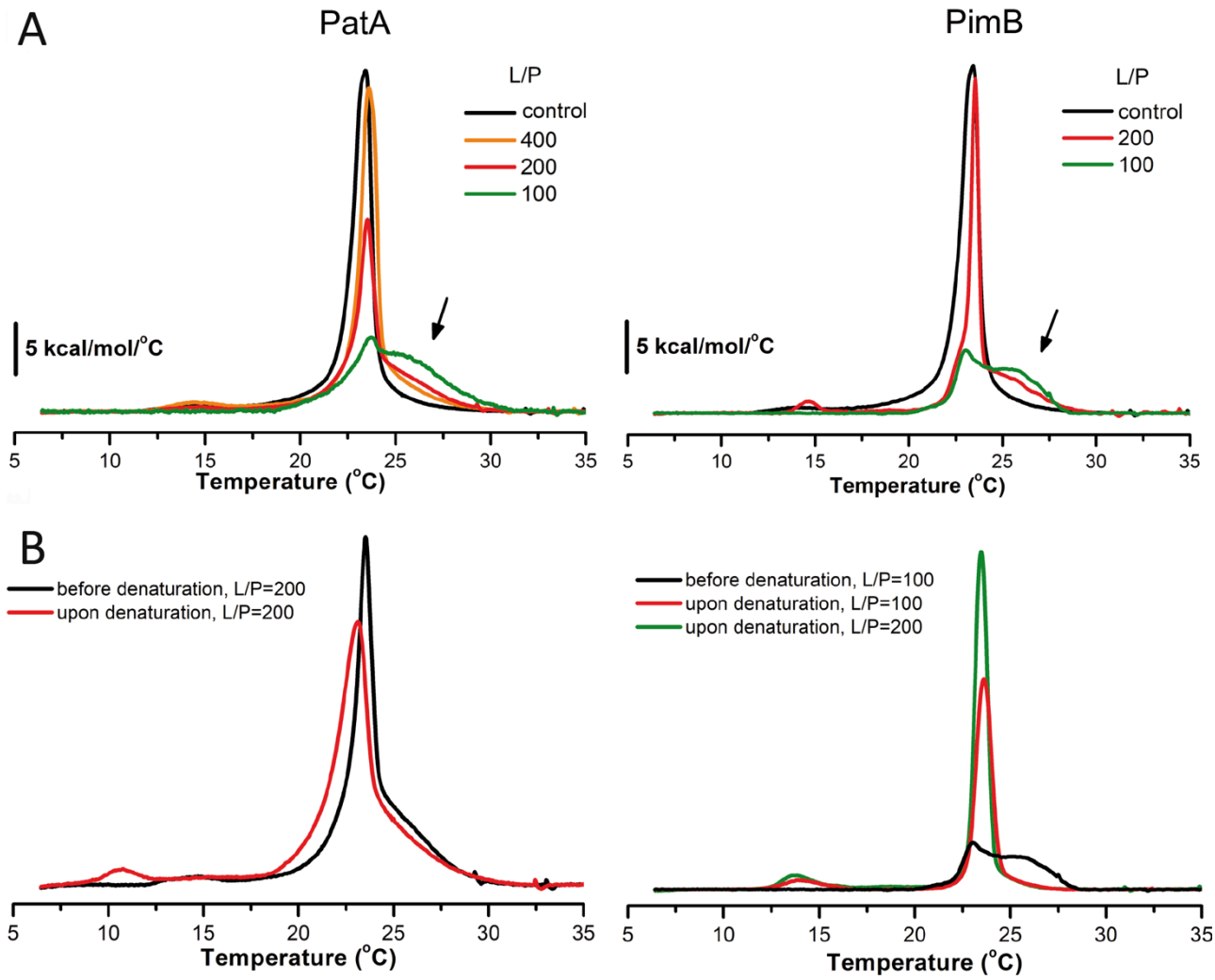

Fig. S4. Effect of the enzymes in the thermodynamics of lipid phase transitions of DMPG/DMPC 40:60 (mol/mol) LUVs. **(A)** Excess heat capacity profiles of the lipid vesicles in the absence (black) and presence of PatA (left) and PimB (right) at the lipid-to-protein molar ratio (L/P) indicated. **(B)** DSC thermograms of the PatA-associated (left) and PimB-associated (right) LUVs recorded before and after protein denaturation.

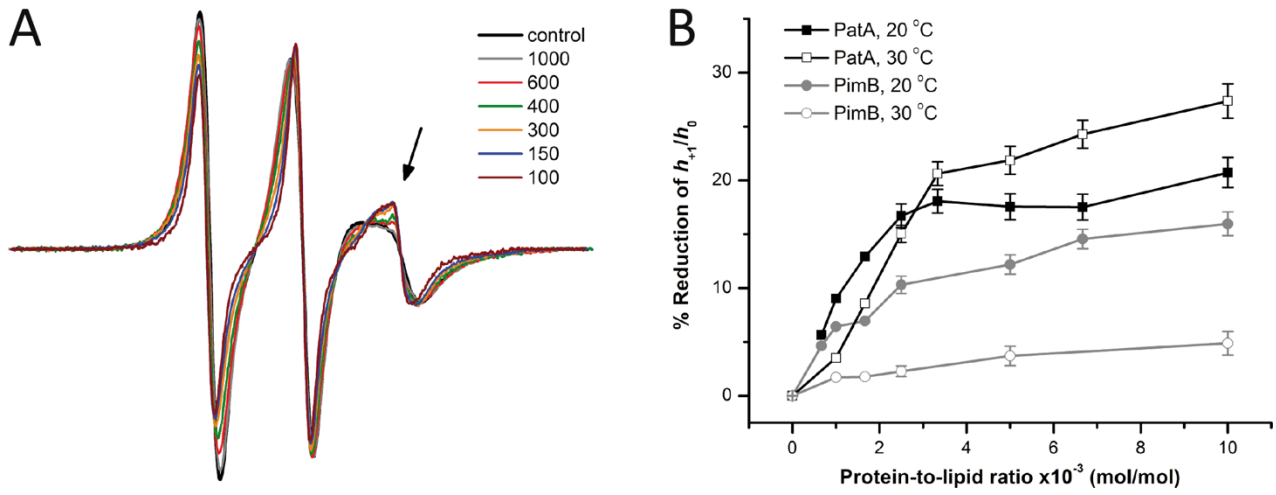

Fig. S5. PatA changes the structural dynamics of DMPG headgroup region more effectively than PimB. (A) DPPTC ESR spectra acquired at 30 ºC in the absence (black line) and presence of PatA at different lipid-to-protein molar ratios (colored lines). The arrow indicates a sharp component. The spectra were normalized by the height of the middle line (h_0). Spectral width is 100 Gauss. **(B)** Percentage reduction of the ratio between the intensity of the low (h_{+1}) and the central (h_0) field lines as a function of the PimB- or PatA-to-lipid molar ratio determined from the DPPTC spectra acquired at the gel (20 ºC) and fluid (30 ºC) phases of DMPG-SUVs.

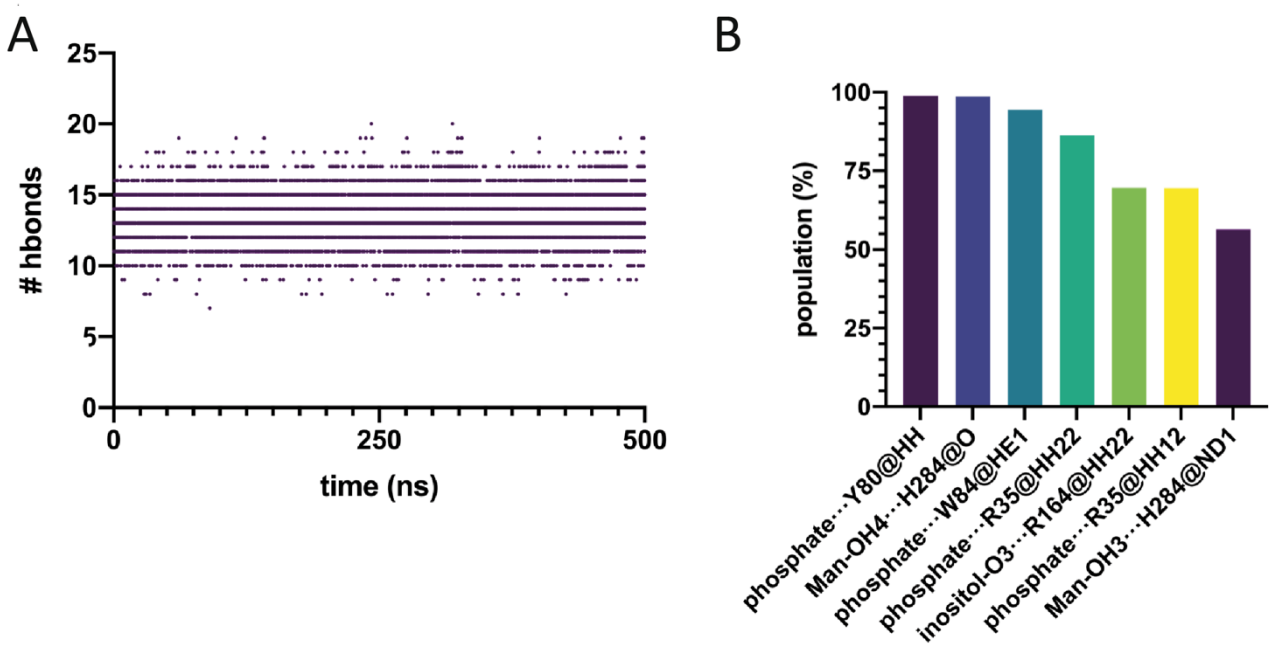

Fig. S6. MD simulations on Ac_1PIM_2/PatA complex embedded in one leaflet of the bilayer. (A) Number of hydrogen bonds found between PatA and the membrane derived from 0.5 μs MD simulations. **(B)** Population (%) of the hydrogen bonds formed between PatA and the PIM_2 glycolipid throughout the MD simulations. The AMBER force field nomenclature was used for the amino acids.

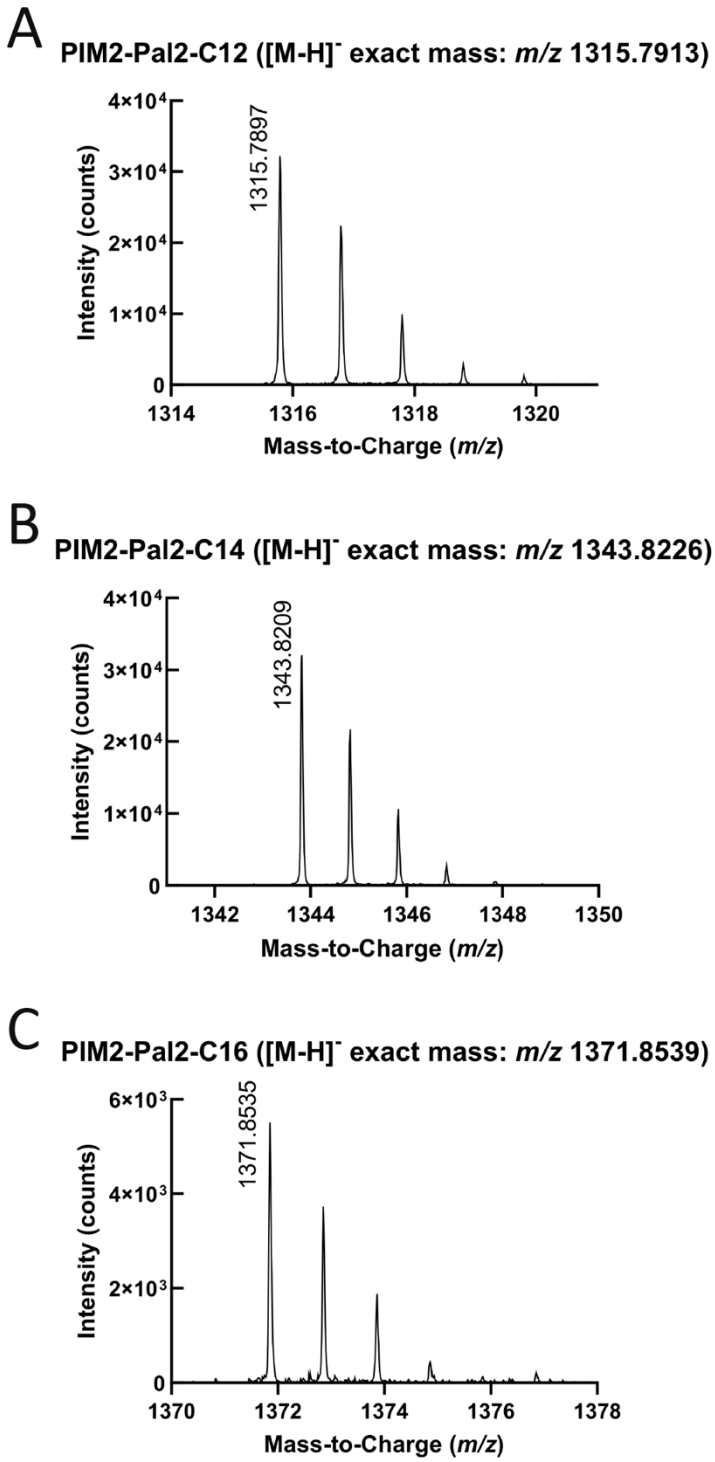

Fig. S7. Representative mass spectra of the deprotonated molecules. (**A**) PIM_2-Pal2-C12 ([M-H]–), (**B**) PIM_2-Pal2-C14 ([M-H]–) and (**C**) PIM_2-Pal2-C16 ([M-H]–).

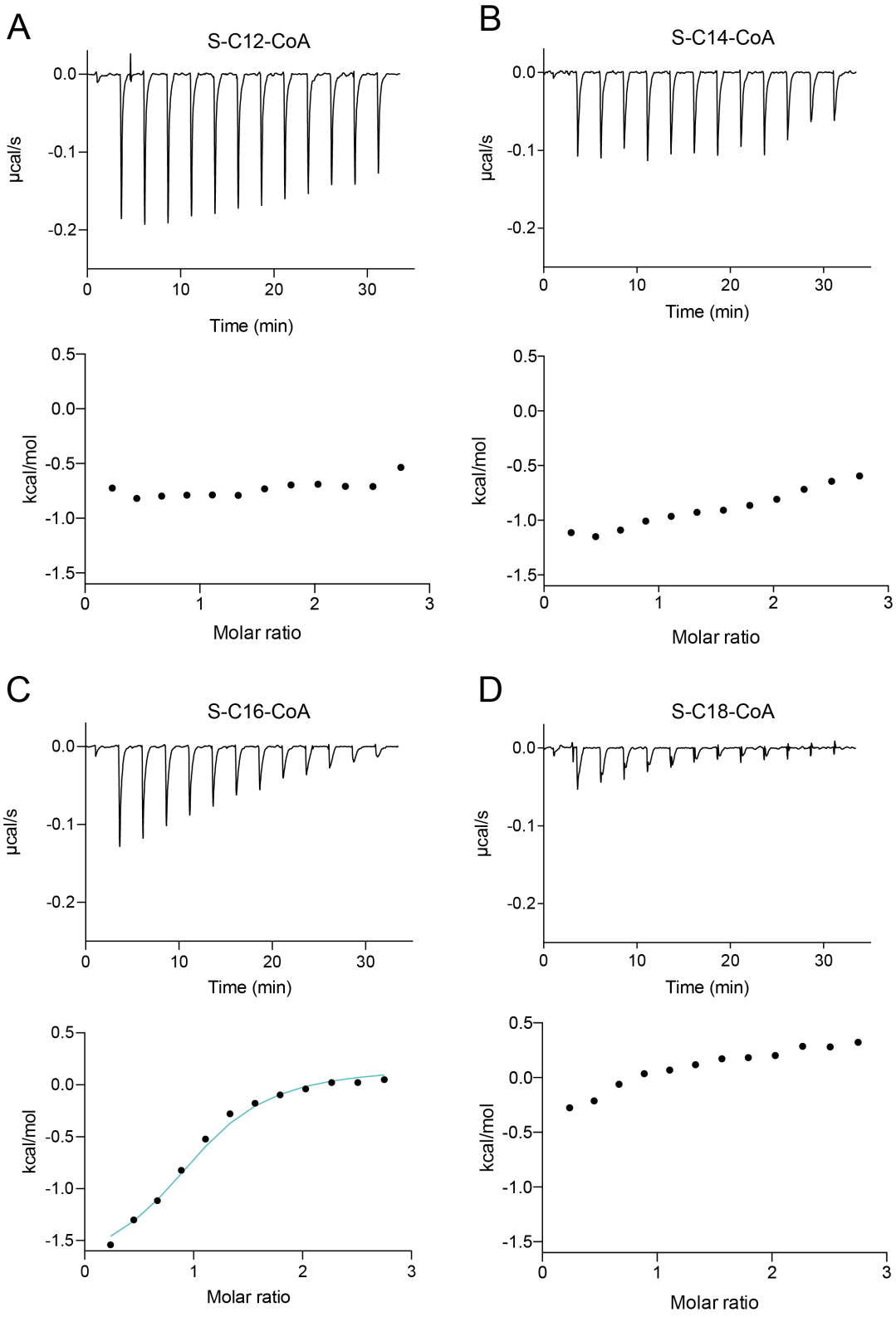

Fig. S8. Acyl chain length binding experiments by ITC. ITC raw and integrated data for PatA and non-hydrolysable acyl-CoA derivatives **(A)** S-C12-CoA **(B)** S-C14-CoA **(C)** S-C16-CoA and **(D)** S-C18-CoA. The experimental points are represented as filled squares and the best fit of these points to a one-site binding model is represented as a solid curve for S-C16-CoA experiment.

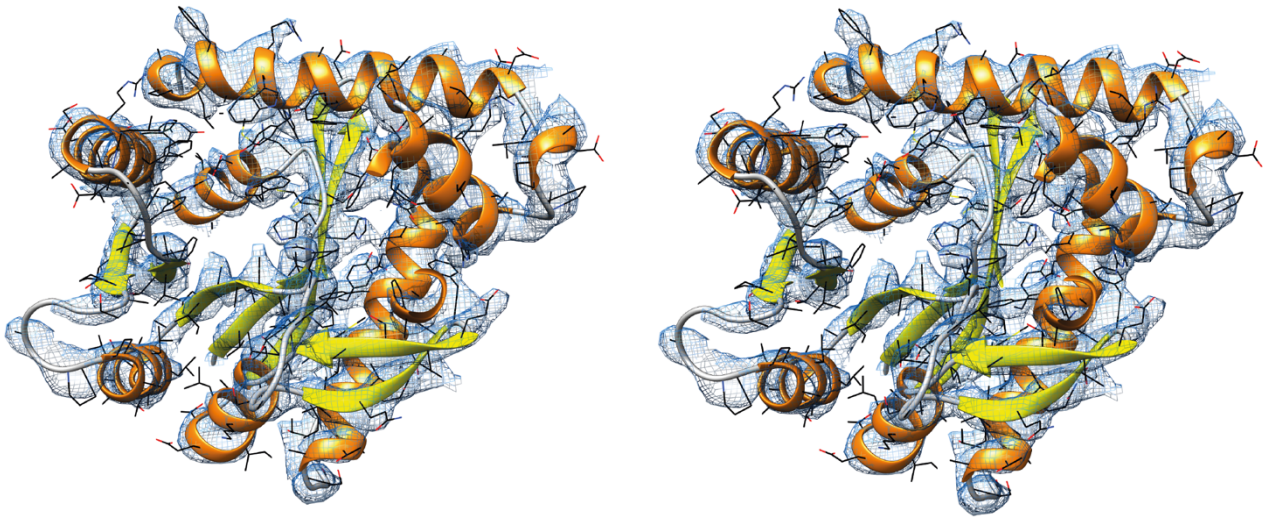

Fig. S9. Electron density map of the refined full length PatA. Stereo view of the final electron density maps (2mFo-DFc contoured at 1σ) corresponding to the full length PatA structure.

Supplementary Tables

Table S1. **Thermodynamic parameters of protein unfolding by CD spectroscopy.** The melting temperature (T_m) and the apparent enthalpy change (ΔH_{app}) for PatA and PimB in the absence and presence of lipids were determined by fitting the CD data to a simple, two-state equilibrium between folded and unfolded states without heat capacity changes, taking into account the pre- and post-transition linear changes in ellipticity as a function of temperature (ref. 40 from main text). The apparent entropy change (ΔS_{app}) of the unfolding transition was calculated as $\Delta S_{app} = \Delta H_{app} / T_m$, since $\Delta G = 0$ at T_m.

Sample	L/P	T_m (ºC)	ΔH_{app} (kcal/mol)	ΔS_{app} (cal/mol.K)
PatA				
No lipid	–	54.0 ± 0.2	86 ± 4	264 ± 12
DOPC/DOPG	10	52.9 ± 0.2	86 ± 5	263 ± 15
DOPC/DOPG	200	55.8 ± 0.2	97 ± 7	293 ± 20
DMPC/DMPG	200	55.1 ± 0.2	105 ± 7	320 ± 22
PimB				
No lipid	–	49.3 ± 0.1	114 ± 3	355 ± 8
DOPC/DOPG	10	49.8 ± 0.1	110 ± 3	340 ± 9
DOPC/DOPG	200	51.9 ± 0.2	67 ± 3	206 ± 8
DMPC/DMPG	200	52.7 ± 0.4	50 ± 4	153 ± 9

Table S2.**Thermodynamic parameters associated to the DMPC/DMPG 40:60 (mol/mol) LUVs phase transitions in the presence of PatA and PimB at different lipid-to-protein (L/P) ratios.** T_p and T_m are, respectively, the temperatures of the pretransition and the gel-to-liquid crystalline phase transition of the lipid samples. In the two-component thermograms of the protein-containing samples, the T_m represents the temperature where the curve reaches its maximum value. The calorimetric enthalpy change, ΔH_{cal}, was calculated as the area under the whole heat capacity curve. $\Delta T_{1/2}$ corresponds to the linewidth at half height of the main, more intense peak. The second scan of the protein-containing samples corresponds to the thermogram recorded after protein denaturation.

Sample	L/P	T_p (ºC)	T_m (ºC)	ΔH_{cal} (kcal/mol)	$\Delta T_{1/2}$ (ºC)
Control					
scan #1	–	14.1	23.4	5.5 ± 0.1	1.1
scan #2	–	14.1	23.5	5.3 ± 0.2	1.1
+ PatA					
scan #1	400	14.4	23.6	5.4 ± 0.1	1.0
scan #2	400	11.6	23.6	5.3 ± 0.2	1.4
scan #1	200	14.7	23.5	4.0 ± 0.2	1.0
scan #2	200	10.6	23.1	4.5 ± 0.3	1.8
scan #1	100	–	23.7	3.4 ± 0.3	4.6
scan #2	100	–	23.8	2.3 ± 0.6	5.6
+ PimB					
scan #1	200	14.6	23.6	3.6 ± 0.2	0.5
scan #2	200	13.8	23.5	4.4 ± 0.3	0.8
scan #1	100	–	23.0	2.2 ± 0.4	4.2
scan #2	100	14.1	23.6	3.3 ± 0.4	1.0

Uncertainties: T_p (± 0.4 ºC), T_m (± 0.1–0.3 ºC), $\Delta T_{1/2}$ (± 0.2–0.4 ºC)

Table S3. Summary of the best-fit NLLS parameters obtained from the simulations of the DPPTC ESR spectra. Best-fit rotational diffusion rate perpendicular to the lipid axis ($R_\perp$), rotational correlation time (τ), order parameters (S_0, S_2), and A_{zz} component obtained from NLLS simulations of the DPPTC ESR spectra in DMPC/DMPG 40:60 (mol/mol) SUVs at 30 ºC in the absence and presence of PatA and PimB at different lipid-to-protein molar ratios (L/P).

System	*L/P*	*comp*	$R_\perp$ ($\times 10^7$ s^{-1})	τ (ns)	S_0	S_2	A_{zz} (G)
control	–	1	3.72	2.27	0.430	-0.091	35.0
+ PatA	1000	1 (99.2%)	4.07	2.24	0.482	-0.098	35.2
		2 (0.8%)	23.9	0.32	0.128	–	37.9
	600	1 (97.2%)	4.79	2.01	0.477	-0.085	35.8
		2 (2.8%)	23.9	0.32	0.128	–	37.9
	400	1 (94.8%)	5.13	1.92	0.391	-0.019	36.3
		2 (5.2%)	23.9	0.32	0.128	–	37.9
	300	1 (92.0%)	6.76	1.43	0.324	0.046	37.0
		2 (8.0%)	23.4	0.33	0.128	–	37.9
	200	1 (91.0%)	7.08	1.35	0.310	0.047	37.1
		2 (9.0%)	22.4	0.33	0.128	–	37.9
	150	1 (86.8%)	7.24	1.12	0.226	0.124	37.3
		2 (13.2%)	20.4	0.36	0.128	–	37.9
	100	1 (77.2%)	7.41	1.08	0.160	0.160	37.3
		2 (22.8%)	25.1	0.41	0.128	–	37.9
+ PimB	1000	1	3.31	2.61	0.447	-0.111	35.0
	600	1	3.16	2.69	0.451	-0.121	35.0
	400	1	3.09	2.72	0.457	-0.142	35.0
	200	1	3.02	2.76	0.459	-0.150	35.0
	100	1	2.95	2.83	0.458	-0.167	35.0

- The uncertainties of the parameters $R_\perp$, τ, S_0, and A_{zz} were estimated in 5%, 2%, 5%, 0.005–0.02, and 0.3 G, respectively.
- The magnetic tensor components of DPPTC were g_{xx}= 2.0086, g_{yy} = 2.0065, g_{zz} = 2.0020, and A_{xx} = A_{yy} = 6.0.

Table S4. Target masses from LC-MS measurement.

Compound class	Compound name	Acronym	Molecular formula	m/z $[M-H]^-$
Fatty acid	**Caprylic acid**	C8:0	$C_8H_{16}O_2$	**143.1078**
Fatty acid	**Lauric acid**	C12:0	$C_{12}H_{24}O_2$	**199.1704**
Fatty acid	**Myristic acid**	C14:0	$C_{14}H_{28}O_2$	**227.2017**
Fatty acid	**Palmitic acid**	C16:0	$C_{16}H_{32}O_2$	**255.233**
Fatty acid	**Stearic acid**	C18:0	$C_{18}H_{36}O_2$	**283.2643**
Fatty acid	**Arachidic acid**	C20:0	$C_{20}H_{40}O_2$	**311.2956**
CoA	**Coenzyme A (CoA)**	CoA	$C_{21}H_{36}N_7O_{16}P_3S$	**766.1079**
CoA derivatives	**Acetyl-CoA**	C2-CoA	$C_{23}H_{38}N_7O_{17}P_3S$	**808.1185**
CoA derivatives	**Octanoyl-CoA**	Capryloyl-CoA(C8-CoA)	$C_{29}H_{50}N_7O_{17}P_3S$	**892.2124**
CoA derivatives	**Dodecanoyl-CoA**	Lauroyl-CoA(C12-CoA)	$C_{33}H_{58}N_7O_{17}P_3S$	**948.275**
CoA derivatives	**Tetradecanoyl-CoA**	Myristoyl-CoA(C14-CoA)	$C_{35}H_{62}N_7O_{17}P_3S$	**976.3063**
CoA derivatives	**Hexadecanoyl-CoA**	Palmitoyl-CoA(C16-CoA)	$C_{37}H_{66}N_7O_{17}P_3S$	**1004.3376**
CoA derivatives	**Octodecanoyl-CoA**	Stearoyl-CoA(C18-CoA)	$C_{39}H_{70}N_7O_{17}P_3S$	**1032.3689**
CoA derivatives	**Eicosanoyl-CoA**	Arachidoyl-CoA(C20-CoA)	$C_{41}H_{74}N_7O_{17}P_3S$	**1060.4002**
PIM2 products	**PIM2-Pal2**	(Substrate)	$C_{53}H_{99}O_{23}P$	**1133.6242**
PIM2 products	**PIM2-Pal2-C2**	(Product)	$C_{55}H_{101}O_{24}P$	**1175.6348**
PIM2 products	**PIM2-Pal2-C8**	(Product)	$C_{61}H_{113}O_{24}P$	**1259.7287**
PIM2 products	**PIM2-Pal2-C12**	(Product)	$C_{65}H_{121}O_{24}P$	**1315.7913**
PIM2 products	**PIM2-Pal2-C14**	(Product)	$C_{67}H_{125}O_{24}P$	**1343.8226**
PIM2 products	**PIM2-Pal2-C16**	(Product)	$C_{69}H_{129}O_{24}P$	**1371.8539**
PIM2 products	**PIM2-Pal2-C18**	(Product)	$C_{71}H_{133}O_{24}P$	**1399.8852**
PIM2 products	**PIM2-Pal2-C20**	(Product)	$C_{73}H_{137}O_{24}P$	**1427.9165**

Table S5. Data collection and Refinement Statistics.

PatA	
Wavelength	0.97625
Resolution range	40.65 - 3.67 (3.80 - 3.67)
Space group	P 1 21 1
Unit cell	81.31 92.97 81.09 90 90.33 90
Total reflections	90742 (7983)
Unique reflections	13263 (1233)
Multiplicity	6.8 (6.5)
Completeness (%)	99.07 (94.90)
Mean I/sigma(I)	9.96 (1.41)
Wilson B-factor	125.8
R-merge	0.1792 (1.459)
R-meas	0.194 (1.584)
R-pim	0.07376 (0.6112)
CC1/2	0.998 (0.7)
CC*	0.999 (0.908)
Reflections used in refinement	13216 (1229)
Reflections used for R-free	660 (62)
R-work	0.2676 (0.3608)
R-free	0.2837 (0.4449)
CC(work)	0.936 (0.737)
CC(free)	0.906 (0.580)
Number of non-hydrogen atoms	7126
macromolecules	7120
ligands	14
Protein residues	996
RMS(bonds)	0.003
RMS(angles)	0.79
Ramachandran favored (%)	98.08
Ramachandran allowed (%)	1.92
Ramachandran outliers (%)	0.00
Rotamer outliers (%)	0.00
Clashscore	6.41
Average B-factor	124.55
macromolecules	124.55
ligands	118.29

Statistics for the highest-resolution shell are shown in parentheses